ACS Macro Letters

Letter

pubs.acs.org/macroletters

Studying Twin Samples Provides Evidence for a Unique Structure-Determining Parameter in Simplifed Industrial Nanocomposites

Guilhem P. Baeza,[†,‡] Anne-Caroline Genix,*[,†,§] Christophe Degrandcourt,[‡] Jérémie Gummel,[∥] Anas Mujtaba,[⊥] Kay Saalwächter,[⊥] Thomas Thurn-Albrecht,[⊥] Marc Couty,[‡] and Julian Oberdisse[†,§]

[†]Université Montpellier 2, Laboratoire Charles Coulomb UMR 5221, F-34095 Montpellier, France

[‡]Manufacture Française des Pneumatiques MICHELIN - Site de Ladoux, 23 place des Carmes Déchaux, F-63040 Clermont-Ferrand CEDEX 09, France

[§]CNRS, Laboratoire Charles Coulomb UMR 5221, F-34095 Montpellier, France

[∥]European Synchrotron Radiation Facility (ESRF), 6 rue Jules Horowitz, BP 220, F-38043 Grenoble CEDEX 09, France

[⊥]Institut für Physik, Martin-Luther-Universität Halle-Wittenberg, D-06099 Halle (Saale), Germany

Supporting Information

ABSTRACT: The structure of styrene−butadiene (SB) nanocomposites filled with industrial silica has been analyzed using electron microscopy and small-angle X-ray scattering. The grafting density per unit silica surface ρ_{D3} was varied by adding graftable SB molecules. By comparing the filler structures at fixed ρ_{D3} (so-called "twins"), a surprising match of the microstructures was evidenced. Mechanical measurements show that ρ_{D3} also sets the modulus: it is then possible to tune the terminal relaxation time of nanocomposites via the chain length while leaving the modulus and structure unchanged.

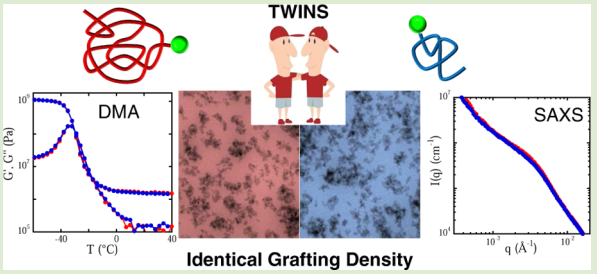

Polymer nanocomposites obtained by blending nanoparticles (NPs) with polymer chains have been recognized to have superior thermomechanical, electrical, or optical properties,[1,2] which may be useless, if these properties cannot be tuned. Some of them, namely, the rheology of filled melts, depend critically on the structure and dispersion of the nanoparticles. It is therefore appealing to control the structure to tailor these properties.

In model nanocomposite systems, i.e., systems containing well-defined colloidal NPs, control parameters for the structure have been evidenced, like the filler volume fraction[3] or the process conditions.[4,5] Large efforts have been devoted to studies of chain structure[6] and dynamics[7] in model systems. In more elaborate systems, adsorbed or grafted NPs have been studied.[8−10] Two additional parameters, the grafting density and the ratio of the grafted-to-matrix chain mass, appear. The dispersion of the NPs and the resulting rheology have been found to depend on both,[10−12] due to a conjunction of factors: the dependence of polymer melt viscosity on chain mass introduces a characteristic time separating a terminal (flow) regime from a plateau modulus at high frequencies.[13] Moreover, grafting chains to a filler skeleton induces a slowing down of the dynamics.[14,15] Finally, the filler contribution depends strongly on the filler structure which may be dispersed, aggregated, or a percolated network[4] and is obviously triggered by the interaction between filler particles, and thus grafting. The detailed structure of the filler particles in industrial nanocomposites has received only little attention,[16−18] presumably due to a complex one-pot formulation in a mixer, a high amount of disorder, and technical difficulties in analyzing the structure. We have recently undertaken a systematic study of the dispersion state of simplified uncross-linked industrial nanocomposites formulated by melt mixing of styrene−butadiene chains with silica of industrial origin, discarding other common ingredients like those related to cross-linking (cf. Supporting Information (SI)). These nanocomposites form by breaking up of silica agglomerates due to the stress mediated by the polymer in the mixer, followed by reaggregation. The latter depends crucially on the details of the NP interactions and is thus determined by the brush structure (see ref 15) and the grafting. We have set up an original structural model based on a quantitative transmission electron microscopy (TEM) and synchrotron small-angle X-ray scattering (SAXS) analysis. Its description for increasing silica volume fraction Φ_{si} extends from the primary silica NPs (of radius ≈10 nm) to NP aggregates (of radius ≈40 nm, compacity ≈35%), up to micrometer-long branches with typical lateral dimension of 150 nm.[19] Furthermore, we have studied the effect of the fraction of graftable matrix chains on the aggregate size.[15] We could show that the aggregate mass can be decreased by about a factor of 4 using grafting. This evolution saturates; i.e., for high enough grafting fractions the structures are the same. The challenge

Received: March 5, 2014
Accepted: April 16, 2014
Published: April 24, 2014

   dx.doi.org/10.1021/mz500137e | ACS Macro Lett. 2014, 3, 448−452

with the data presented up to now is that such a quantitative characterization has to be carried out for each chain mass, for each fraction of graftable chains, and for each silica volume fraction. Due to the chain mass dependence of the viscosity, it is tempting to believe that the final filler structure (after mixing) is determined by the chain mass. It is the ambition of the present letter to show that this is not the case and propose a unique structure-determining parameter for such industrial nanocomposites.

Simplified industrial nanocomposites with precipitated silica and SB chains of different mass (M_{SB} = 40, 80, 140, and 280 kg mol^{-1}, all with polydispersity index below 1.1 given by size exclusion chromatography) have been formulated in an internal mixer. A fraction %$D3$ of the chains is endowed with a single grafting function. Details on the formulation and grafting efficiency are given in the SI. The nominal grafting density of the polymer chains on the available silica surface reads

$$\rho_{D3} = \frac{(1 - \Phi_{si})N_A \%D_3 d_{SB} R_0 \exp(2.5\sigma^2)}{3M_{SB}\Phi_{si}} \quad (1)$$

where d_{SB} = 0.94 g cm^{-3} is the density of the polymer; R_0 = 8.55 nm and σ = 0.27 are the log-normal silica bead parameters; and N_A is the Avogadro number. Equation 1 gives the number of grafting functions per unit NP surface calculated with the average surface and volume deduced from the log-normal NP size distribution. Note that some 80% of the NPs are located at the surface of a typical aggregate (radius 50 nm, compacity 35%), implying that they offer a large part of their surface for grafting due to the noncompact aggregate density. The nominal grafting density is thus a reasonable estimate of the real one. In our forthcoming paper,[20] deviations between the nominal NP grafting and the grafting on the aggregate surface have been used to construct a physical model reproducing the size dependence of aggregates. For a given filler surface area, the grafting density ρ_{D3} increases with the %$D3$ fraction and decreases as the chain mass goes up, due to the obvious scarcity of chain ends. In a forthcoming article,[20] we will show that higher chain masses at fixed matrix composition (50%$D3$) lead to bigger aggregates, an effect opposite to higher grafting. The latter two dependencies together suggest checking the pertinence of the ρ_{D3}-parameter as a control parameter of aggregate structure. We now focus on the impact of ρ_{D3} on the filler structure as seen by SAXS in the intermediate q-range. SAXS experiments were performed on beamline ID2 (ESRF, Grenoble, cf. SI). In the course of this project, more than 100 samples have been formulated, varying the silica volume fraction (five values from Φ_{si} = 0 to 20%), the chain mass (four masses from 40 to 280 kg mol^{-1}), and the matrix composition (five fractions from 0 to 100%$D3$). For these samples, we have calculated the grafting density ρ_{D3} and identified couples with ρ_{D3} as close as possible. In some cases, e.g., a doubled mass compensated by doubled grafting, the comparison may be exact. The Φ_{si} values determined by TGA are slightly scattered, which is luckily without consequences because aggregate structures depend weakly on Φ_{si}.[19] In Table 1, the parameters of the available ρ_{D3}-twin nanocomposite couples with ρ_{D3} within $\pm 2 \times 10^{-3}$ nm^{-2} are reported. In Figure 1, two comparisons (low and high Φ_{si}) between intensities for twin nanocomposites with $\rho_{D3} = 35$ and 51×10^{-3} nm^{-2} are shown. Others, from ρ_{D3} = 0 to 71×10^{-3} nm^{-2}, are given in the SI. At low silica volume fraction (≈9%), the increase in chain mass from 140 to 280 kg mol^{-1} is compensated by the increase in %$D3$. ρ_{D3} equals ≈35×10^{-3} nm^{-2} for both, and the intensities superimpose in a satisfying manner over almost the entire q-range.

Table 1. ρ_{D3} Twin Samples with Different Formulation Parameters[a]

	twin sample 1			twin sample 2		
ρ_{D3}	M_{SB}		Φ_{si}	M_{SB}		Φ_{si}
[10^{-3} nm^{-2}]	[kg mol^{-1}]	%D_3	[% vol]	[kg mol^{-1}]	%D_3	[% vol]
0	140	0	16.7	40	0	20.4
0	140	0	8.6	280	0	9.6
16	140	25	16.8	280	50	19.4
35	140	25	8.6	280	50	9.5
51	40	25	18.9	80	50	19.5
71	140	50	8.4	280	100	9.5

[a]The nominal grafting densities ρ_{D3} of such samples are as close as possible (within 2×10^{-3} nm^{-2}, except for the last twin: $\pm 4 \times 10^{-3}$ nm^{-2}).

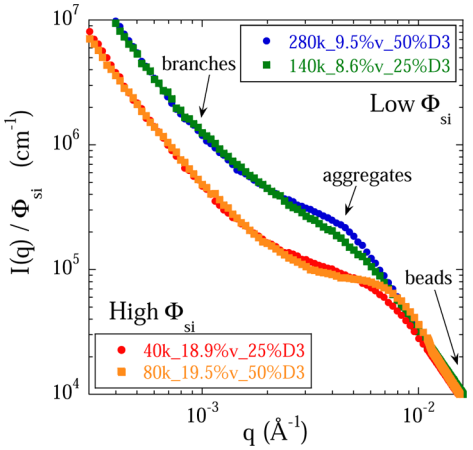

Figure 1. Comparison of silica structure studied by SAXS in ρ_{D3}-twin nanocomposites. Low Φ_{si}: $\rho_{D3} = 37 \times 10^{-3}$ nm^{-2}, 140 kg mol^{-1}, 25% $D3$ vs $\rho_{D3} = 33 \times 10^{-3}$ nm^{-2}, 280 kg mol^{-1}, 50%$D3$. High Φ_{si}: $\rho_{D3} = 52 \times 10^{-3}$ nm^{-2}, 40 kg mol^{-1}, 25%$D3$ vs $\rho_{D3} = 50 \times 10^{-3}$ nm^{-2}, 80 kg mol^{-1}, 50%$D3$. Arrows indicate the zones corresponding to different structural levels.

A similar comparison is performed for a higher volume fraction (≈19%), with 40 and 80 kg mol^{-1}, leading to $\rho_{D3} \approx 51 \times 10^{-3}$ nm^{-2}. Again the superposition of the intensities is remarkable, suggesting a very similar filler structure on this scale. However, to be more quantitative, one needs to compare the differences between the intensities to some norm. We have chosen the evolution of the intensities as a function of %$D3$ at fixed mass for comparison because there the whole range from widely different structures (i.e., typically a factor of 4 between aggregation numbers) to identical ones is covered. The assessment of the difference between two intensities I and I_{ref} normalized to their respective Φ_{si} is then done by calculating the following deviation integral DI

$$\mathrm{DI} = \int_{q_{min}}^{q_{max}} \left[\frac{I(q)}{I_{ref}(q)} - 1\right]^2 d\log(q) \quad (2)$$

where q is measured in Å^{-1}. DI is constructed as the integral over a square to define a positive distance between curves. In Figure 2, two examples of the integrand $(I/I_{ref} - 1)^2$ are shown as a function of q. The original intensities are shown in the

dx.doi.org/10.1021/mz500137e | ACS Macro Lett. 2014, 3, 448−452

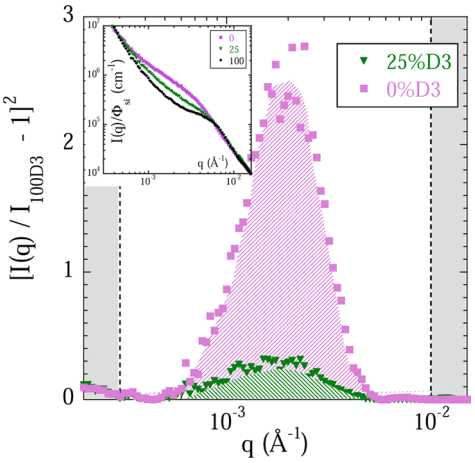

Figure 2. Quantification of the deviation between filler structures using the intensity ratio for 0%, 25%, and 100%*D*3 (140 kg mol^{-1}, ≈9% vol silica). The integral DI calculated as the shaded area decreases as the SAXS intensities shown in the inset become closer to the 100%*D*3 data.

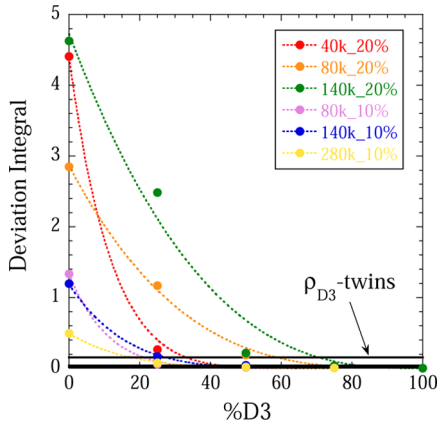

Figure 3. DI measuring the deviation between filler structures, for families of curves as indicated in the legend, vs %*D*3. Dotted lines are a guide to the eye. The DI values of the ρ_{D3} twins given in Table 1 are plotted as black lines at the bottom. They range from 0.021 to 0.155, the highest one being the 71 × 10^{-3} nm^{-2} twin.

inset. The three curves correspond to 0%, 25%, and 100%*D*3 (140 kg mol^{-1}, 9% silica) and evolve progressively toward the limiting curve at 100%*D*3,[15] which is taken as the reference curve I_{ref} in eq 2. The resulting integral between the limits indicated in the graph gives 1.19 and 0.16, respectively. The choice of the q limits—fixed for all samples—is explained in the SI. The narrowing of the deviation at intermediate angles in the inset is thus translated correctly first in the curves shown in Figure 2 and then into a value corresponding to the area under that curve. Obviously, strictly identical $I(q)$ and $I_{ref}(q)$ yield the minimum value of DI, which is zero for 100%*D*3. Note that these results are robust: we have checked that integrating over dq instead of $d\log(q)$ shifts the numerical values but does not affect the results.

Equation 2 thus gives us a tool to compare deviations between intensity curves in a quantitative manner. To explore the full range, we have calculated integral values DI for several families of curves of varying matrix composition %*D*3 from 0 to 100%: at 40 (Φ_{si} = 20%), 80 (10%; 20%), 140 (10%; 20%), and 280 kg mol^{-1} (10%). We have always chosen I_{ref} to be at 100% *D*3. The comparison between the DI values of these families and the ρ_{D3} twin samples given in Table 1 (ρ_{D3} = 0−71 × 10^{-3} nm^{-2}) is shown in Figure 3. Within a family, the fact that the intensity curves approach as %*D*3 increases is reflected by the decrease of the integral DI to zero. The DI values of all ρ_{D3} twins obtained by taking one of them as I_{ref} are shown as solid lines at the bottom of the plot. These DI values are clearly considerably smaller than all others, confirming now quantitatively that the resemblance of the graphs in Figure 1 is not only a visual effect. Finally, it may be noted that the similarity observed here is fundamentally different from the saturation effect described in ref 15, where we have shown that the structure of samples does not evolve above a critical grafting value. In the present letter, the similarity holds for arbitrary grafting densities of twins. Note that due to the similar size of aggregates, a possible deviation between nominal and real grafting density caused by inaccessible inner NPs would be very similar for each twin.

As a next step, we have compared filler structures by TEM. The pictures of the low-Φ_{si} twin samples (35 × 10^{-3} nm^{-2}) compared in Figure 1 are confronted in Figures 4(a) and (b). If it were not for the slight difference in luminosity, one could think the two pictures were parts of one bigger one. The agreement is striking and confirms the findings of the SAXS study: samples of identical grafting density ρ_{D3} but with highly different chain mass and thus mixing viscosity display the same filler structure (see SI for another example). For comparison, at low ρ_{D3}, the structure is significantly different, as can be seen in Figure 4(c).

One of the fundamental questions of nanocomposites is to understand and control the influence of the structure on the mechanical properties. We have used DMA (see SI) to measure the storage and loss moduli of twins (cf. Figure 5). The result for the ρ_{D3} twins with (35 ± 2) × 10^{-3} nm^{-2} (cf. Table 1) measured at 10 Hz is shown in the inset of Figure 5. The curves have the classical appearance of moduli, with a maximum due to the segmental relaxation in $G''(T)$ and a glassy plateau at low temperatures. Above the glass transition, the viscoelastic (rubbery) plateau is found. For comparison with previous shear experiments (150 Hz) at 50 °C, in which this plateau appeared at high frequencies,[15,19] we have used the time−temperature superposition principle[13] and report corresponding DMA moduli at 2 °C and 10 Hz in Figure 5, for the samples in Table 1. Clearly, the plateau moduli are identical within 10% for each twin. At 10% vol silica, they are close for all samples, whereas at 20% vol a strong decrease is observed with increasing ρ_{D3}, proving the tunability of the performance at high filler fraction. Twins have thus an identical structure and storage plateau modulus but display different dynamics in the terminal regime, due to the widely different chain masses. For the twins at ρ_{D3} = 35 × 10^{-3} nm^{-2}, we have checked that their characteristic time evolves from 2.4 to 23.1 s, in quantitative agreement with changes in mass by a factor of 2 inducing a change in time by $2^{3.4}$ = 10.5.[21]

In conclusion, we have proposed robust evidence for the existence of a unique control parameter, the grafting density ρ_{D3}, in simplified industrial nanocomposites. Note that in model systems similar morphology-determining parameters have been identified.[22] This parameter determines the filler structure as evidenced by SAXS and TEM on twins, defined by different mass and grafting, but identical ρ_{D3}. The physical mechanism relating grafting density and structure formation in the mixer may be considered. Given the generally high grafting

dx.doi.org/10.1021/mz500137e | ACS Macro Lett. 2014, 3, 448−452

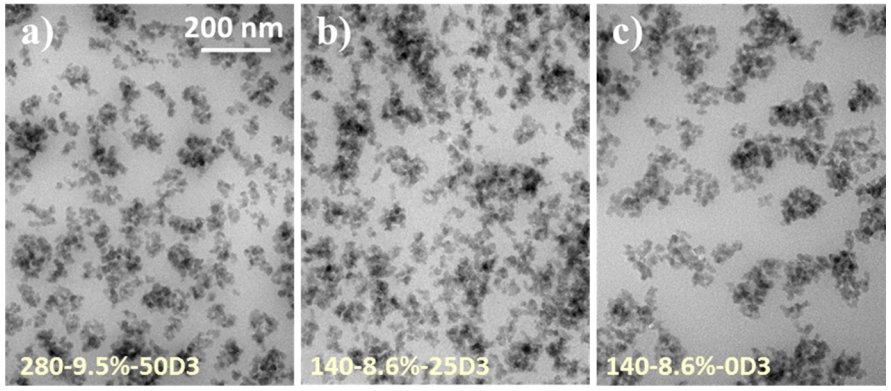

Figure 4. (a) and (b): TEM of ρ_{D3} twin nanocomposites with close grafting density $\rho_{D3} = (35 \pm 2) \times 10^{-3}$ nm^{-2}. Silica volume fraction ≈9% vol, 140 kg mol^{-1}, 25%*D*3, and 280 kg mol^{-1}, 50%*D*3. For comparison (c) $\rho_{D3} = 0$ nm^{-2} with 140 kg mol^{-1}, 0%*D*3.

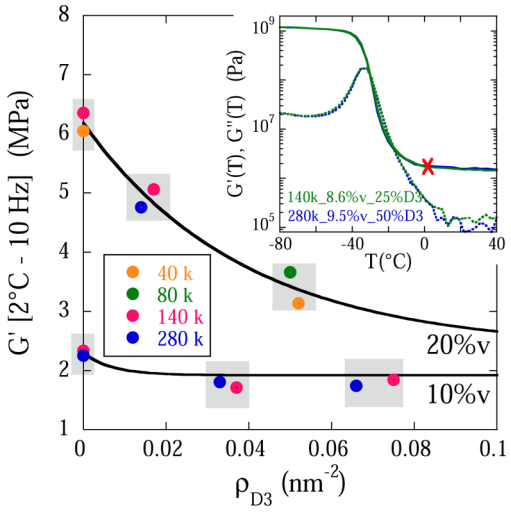

Figure 5. Viscoelastic plateau moduli at 2 °C/10 Hz from DMA for all twin samples (see legend for chain masses). In the inset, the complete DMA curves (G' solid, G'' dotted line) are plotted for a silica volume fraction ≈9% vol, 140 kg mol^{-1}, 25%*D*3, and 280 kg mol^{-1}, 50%*D*3 ($\rho_{D3} = (35 \pm 2) \times 10^{-3}$ nm^{-2}). Shadowed areas identify twins.

densities, layers are necessarily dense with little matrix chain interpenetration, in particular as matrix and graft chain masses are identical ("dry" layer). Such layers favor steric stabilization of filler aggregates. During mixing, aggregates break up and reagglomerate if this is not impeded by dense enough grafting at their surface, which is size dependent. Higher grafting densities thus lead to smaller objects. An empirical model of size as a function of grafting density will be proposed in the future. In this respect, the mass of the grafts is irrelevant as it affects only the layer thickness (which is already considerable with 40 kg mol^{-1}), not the layer density, thus conferring identical structures to twins. The mechanical properties of such twins are characterized by an identical viscoelastic plateau and thus reinforcement. Moreover, the latter is tunable with ρ_{D3} at 20% vol silica. Finally, it is possible to control the onset of the terminal flow behavior of twin samples over a wide frequency range by modifying the chain mass at fixed ρ_{D3}. It is believed that both the evidence for structure control and the strategy of structural analysis reported here for highly disordered systems will be of relevance for a general class of disordered materials, including both industrial and model nanocomposites.

■ ASSOCIATED CONTENT

Ⓢ Supporting Information

Experimental details and additional data regarding structure and mechanics for the twins. This material is available free of charge via the Internet at http://pubs.acs.org.

■ AUTHOR INFORMATION

Corresponding Author

*E-mail: acgenix@univ-montp2.fr.

Notes

The authors declare no competing financial interest.

■ ACKNOWLEDGMENTS

We are thankful for a Chercheur d'Avenir grant by the Languedoc–Roussillon region (J.O.) and Ph.D. funding CIFRE (G.P.B.).

■ REFERENCES

(1) Heinrich, G.; Kluppel, M.; Vilgis, T. A. *Curr. Opin. Solid State Mater. Sci.* **2002**, *6* (3), 195–203.
(2) Jancar, J.; Douglas, J. F.; Starr, F. W.; Kumar, S. K.; Cassagnau, P.; Lesser, A. J.; Sternstein, S. S.; Buehler, M. J. *Polymer* **2010**, *51* (15), 3321–3343.
(3) Jouault, N.; Vallat, P.; Dalmas, F.; Said, S.; Jestin, J.; Boue, F. *Macromolecules* **2009**, *42* (6), 2031–2040.
(4) Oberdisse, J. *Soft Matter* **2006**, *2* (1), 29–36.
(5) Janes, D. W.; Moll, J. F.; Harton, S. E.; Durning, C. J. *Macromolecules* **2011**, *44* (12), 4920–4927.
(6) Crawford, M. K.; Smalley, R. J.; Cohen, G.; Hogan, B.; Wood, B.; Kumar, S. K.; Melnichenko, Y. B.; He, L.; Guise, W.; Hammouda, B. *Phys. Rev. Lett.* **2013**, *110* (19), 196001.
(7) Agarwal, P.; Kim, S. A.; Archer, L. A. *Phys. Rev. Lett.* **2012**, *109* (25), 258301.
(8) Kim, S. Y.; Schweizer, K. S.; Zukoski, C. F. *Phys. Rev. Lett.* **2011**, *107* (22), 225504.
(9) Martin, T. B.; Dodd, P. M.; Jayaraman, A. *Phys. Rev. Lett.* **2013**, *110* (1), 018301.
(10) Kumar, S. K.; Jouault, N.; Benicewicz, B.; Neely, T. *Macromolecules* **2013**, *46* (9), 3199–3214.
(11) Chevigny, C.; Dalmas, F.; Di Cola, E.; Gigmes, D.; Bertin, D.; Bou, F.; Jestin, J. *Macromolecules* **2011**, *44* (1), 122–133.
(12) Hasegawa, R.; Aoki, Y.; Doi, M. *Macromolecules* **1996**, *29* (20), 6656–6662.
(13) Ferry, J. D. *Viscoelastic properties of polymers*; Wiley: New York, 1980.
(14) Reith, D.; Milchev, A.; Virnau, P.; Binder, K. *Macromolecules* **2012**, *45* (10), 4381–4393.

(15) Baeza, G. P.; Genix, A. C.; Degrandcourt, C.; Petitjean, L.; Gummel, J.; Schweins, R.; Couty, M.; Oberdisse, J. *Macromolecules* **2013**, *46* (16), 63886394.
(16) Shinohara, Y.; Kishimoto, H.; Yagi, N.; Amemiya, Y. *Macromolecules* **2010**, *43* (22), 9480−9487.
(17) Choi, S. S.; Kim, I. S.; Lee, S. G.; Joo, C. W. *J. Polym. Sci., Part B: Polym. Phys.* **2004**, *42* (4), 577−584.
(18) Mujtaba, A.; Keller, M.; Ilisch, S.; Radusch, H. J.; Thurn-Albrecht, T.; Saalwachter, K.; Beiner, M. *Macromolecules* **2012**, *45* (16), 6504−6515.
(19) Baeza, G. P.; Genix, A. C.; Degrandcourt, C.; Petitjean, L.; Gummel, J.; Couty, M.; Oberdisse, J. *Macromolecules* **2013**, *46* (1), 317−329.
(20) Baeza G. P. et al., in preparation.
(21) Doi, M.; Edwards, S. F. *The Theory of Polymer Dynamics*; Oxford University Press: Oxford, 1986.
(22) Akcora, P.; Liu, H.; Kumar, S. K.; Moll, J.; Li, Y.; Benicewicz, B. C.; Schadler, L. S.; Acehan, D.; Panagiotopoulos, A. Z.; Pryamitsyn, V.; Ganesan, V.; Ilavsky, J.; Thiyagarajan, P.; Colby, R. H.; Douglas, J. F. *Nat. Mater.* **2009**, *8* (4), 354−U121.